Available online at www.sciencedirect.com

jmr&t Journal of Materials Research and Technology

journal homepage: www.elsevier.com/locate/jmrt

Impact of aging on the sintering behavior of bioactive-glass powder

Andrea Mari [a], *Matteo Pavarini* [a], *Pier Francesco Menci* [a], *Cindy Charbonneau* [b,*], *Louis-Philippe Lefebvre* [b], *Luigi De Nardo* [a]

[a] *Department of Chemistry, Materials and Chemical Engineering "G. Natta", Politecnico di Milano, Milano, 20131, Italy*

[b] *National Research Council Canada, Boucherville, Quebec, J4B 6Y4, Canada*

ARTICLE INFO

Article history:
Received 9 February 2023
Accepted 21 June 2023
Available online 24 June 2023

Keywords:
Bioactive glass
Scaffolds
Glass-ceramic materials
Ageing
Advanced manufacturing

ABSTRACT

Bioactive glasses (BGs) have been successfully used for several years as bone graft substitutes to fill defects and augment bone structures in orthopedic and dental procedures. Despite recent advances in the fabrication of reliable 3D scaffolds based on BG, the reproducibility of fabrication has only been marginally addressed and remains a challenge for their application. Recent studies have shown that BGs can react with moisture and atmospheric CO_2 to form carbonates, affecting the properties and structure of the final product. In this study, factors that can affect the sintering behavior of BG powders were identified and investigated. A statistical analysis was then performed to optimize the BG sintering process, which revealed the possibility of obtaining BG scaffolds with reproducible density by acting on controllable factors such as aging and drying. In practice, this can be achieved by controlling the atmosphere during processing, handling, and storage of the material.

1. Introduction

Bioactive glasses (BGs), such as 45S5 Bioglass and glass ceramics, have been a major focus for bone tissue regeneration since their discovery by L.L. Hench in the late 1960s [1,2]. Upon contact with a biological environment, BGs dissolve and release ions that promote the formation of a biologically active hydroxycarbonate apatite (HCA) layer that mimics the mineral phase of bone [3]. These properties made BGs attractive as a viable alternative to autologous bone grafting in the treatment of traumatic and pathological conditions [4], leading to critical medical applications in the form of granules (BoneAlive®, PerioGlas®, Biogran®), pastes, and putties (NovaBone®, Signafuse®, BioSphere®, NanoFuse®) [5].

Over the past decade, interest in bioactive glass and glass-ceramic structures derived from it has increased, and significant efforts have been made to develop BG-based scaffolds and advanced porous structures for bone tissue engineering [6]. However, these efforts have not resulted in a noticeable increase in the number of devices approved for clinical use with porous structures. One of the main reasons hindering implementation in clinical applications is the challenge of fabricating reproducible and reliable structures on a large scale.

Several studies [7–11] and reviews [3,6,12] have pointed out the importance of adapting the fabrication process to the biological requirements of tissue regeneration [13]. The ideal scaffold should mimic trabecular bone and have balanced mechanical and biodegradation properties to promote complete bone structure repair. The degradation kinetics must be

* Corresponding author. Tel.: +1 450 641 5026
E-mail address: cindy.charbonneau@cnrc-nrc.gc.ca (C. Charbonneau).
https://doi.org/10.1016/j.jmrt.2023.06.204

controlled during the healing process to reduce the inflammatory response and provide a temporary mechanical support [14]. All these aspects either depend on or are strongly influenced by the structural properties of the scaffold, which can be controlled and adjusted by the processing conditions on BGs.

Previous studies have shown that Bioglass® particles are not stable and can react with atmospheric CO_2 in a humid environment to form carbonates (Na_2CO_3 and $CaCO_3$) and hydrocarbonates ($NaHCO_3$) [15,16]. While the *in vitro* and *in vivo* behavior of BG is well documented in the literature [3,6,12], there is little information to date on the effects of these carbonates on the processing of BG powders. For example, the rapid dissolution of carbonate species and the release of ions from BG can affect the pH of the environment, which has non-negligible effects on glass particle suspensions used in toothpaste, cosmetics, or graft substitute putties. A more crucial aspect for Bioglass® solid structures is that the shape, density and concentration of carbonate surface species can vary significantly depending on aging conditions (temperature, humidity, and CO_2 concentration), which affects BG processing (*i.e.*, sintering) and final properties. Therefore, appropriate handling and packaging conditions should be selected to control their formation.

In this study, the effect of aging Bioglass® powders on the formation of carbonates is investigated, focusing on the impact on sintering. The controllable factors affecting the sintering process were evaluated by chemical, physical and morphological characterization of the powders. As a result, an optimized experimental procedure is proposed to maximize the reproducibility of the sintered scaffolds.

2. Materials and methods

2.1. Bioglass® powder

SCHOTT AG supplied Bioglass® powder (Vitryxx® Bioactive Glass, D50: 4.0 ± 1.0 μm particle size) with the following weight composition: $24.5Na_2O–24.5CaO–6P_2O_5–45SiO_2$. The powder was used as supplied unless otherwise stated.

2.2. Aging of BG powder

Five vials with 7g each of BG powder were prepared. One vial was sealed and stored under vacuum as a control sample. Four open vials were subjected to accelerated aging treatment in an incubator (Forma Serie II, Thermo Electron Corporation, Waltham, MA, USA) at 37 °C, 90% relative humidity (RH), and 5% [CO_2] for 1, 2, 4, and 8 weeks. After aging, the samples were oven-dried (ISOTEMP 550D, Fisher Scientific, Hampton, NH, USA) at 100 °C for 24 h to remove residual absorbed water and then vacuum-sealed until further use.

2.3. Preparation of BG pellets

Approximately 2 g of each BG powder sample (control and aged) was rinsed in Milli-Q water (DI H2O, 18 MΩ cm) and centrifuged at 1000 rpm for 30 min (IEC Centra CL2, Thermo Fisher Scientific, Waltham, MA, USA) to remove soluble carbonates that had formed on the surface. The rinsed powders were then isolated and oven dried at 100 °C for 24 h as described above.

The BG powders were successfully pressed into pellets to study their sintering behavior. To produce pellets, approximately 1.3 g of powder was poured into a cylindrical mold with a diameter of 15.8 mm and a pressure of 500 MPa was applied using a 100-ton hand press (RK Machinery, Canada). A zinc stearate lubricant was sprayed onto the mold before each press cycle to facilitate pellet removal. Pellets were prepared from rinsed and unrinsed powders for each aging time point.

2.4. Sintering experiments

The pellets were placed on an alumina plate coated with yttria. The plate containing the samples was positioned in the center of a 6-inch tube furnace (Model 54,753, Lindberg, Riverside, MI, USA). A constant heating rate of 200 °C per hour was set until a temperature of 1035 °C was reached. Sintering was performed at 1035 °C for 1 h in 5 SCFH air. A constant cooling rate of 600 °C per hour was set until the ambient temperature was reached.

2.5. Chemical-physical and morphological characterization of BG powder and pellets

The mass uptake (MU) of BG powder was evaluated at each timepoint to estimate the formation of carbonate species using equation (1):

$$MU(t) = \frac{\omega_d\,(t) - \omega_0}{\omega_0} \times 100 \tag{1}$$

where ω_0 is the initial weight and $\omega_d\,(t)$ is the weight after drying at each aging time t. A carbon determinator (LECO CS600, St Joseph, MI, USA) was used to evaluate carbon uptake. Triplicate measurements were performed for each powder sample.

The evolution of the crystalline phase was followed by X-ray diffraction spectroscopy (XRD, D8 Discover, Bruker, Billerica, MA, USA) with Cu kα radiation. Patterns were recorded in the range of 20°–90° 2θ with a step size of 0.02° and analyzed using DIFFRAC. EVA V2.0 software (Bruker, Billerica, MA, USA).

Moisture content was determined using a Computrac® Vapor Pro® Moisture Analyzer (Ametek, Chandeler, Arizona, USA). For these tests, the powder samples were heated, and the resulting volatiles were passed through an analysis cell where the moisture content of the flowing gas was measured.

The effect of aging on the sintering of BG was evaluated based on variations in the dimensions, weight, and density variations of the pellets. Weight, diameter and thickness were measured for each sample before and after sintering. The respective changes were calculated using equations (2)–(4):

$$\omega_v\,(\%) = \frac{\omega_f - \omega_0}{\omega_0} \times 100 \tag{2}$$

$$d_v\,(\%) = \frac{d_f - d_0}{d_0} \times 100 \tag{3}$$

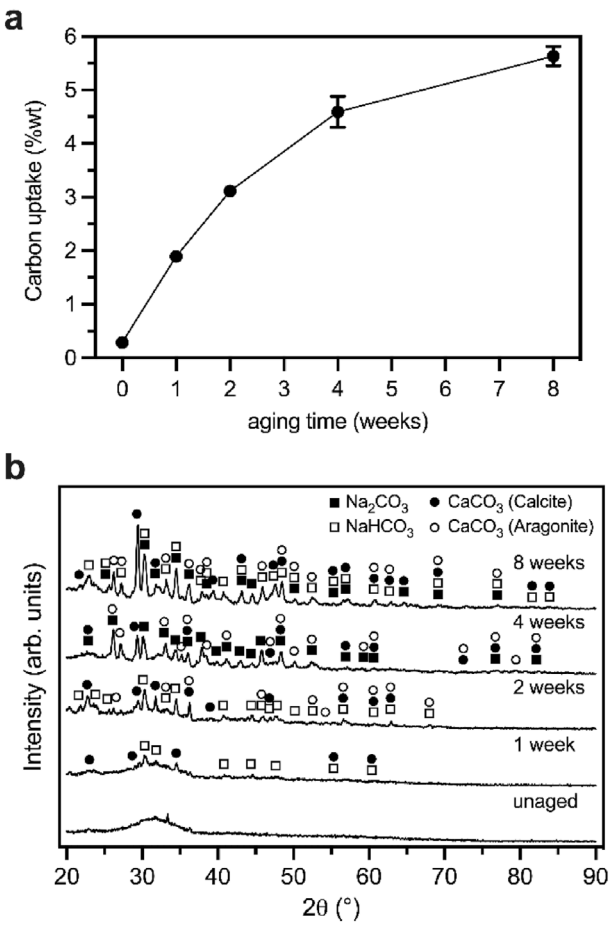

Fig. 1 – Characterization of the powder. (a) Carbon uptake of Bioglass® powders as a function of aging time at 37 °C, 90% RH, and 5% CO_2. (b) XRD patterns of unaged (pristine) and aged (1, 2, 4, and 8 weeks) powders. (■) = Na_2CO_3 (PDF 98-016-8129); (□) = $NaHCO_3$ (PDF 98-001-8183, 98-002-3868 and 98-002-6933); (●) = $CaCO_3$ (Calcite, PDF 98-001-8166, 98-015-8257, and 98-016-9932); (○) = $CaCO_3$ (Aragonite, PDF 98-005-6090 and 98-016-9893).

$$t_v\,(\%) = \frac{t_f - t_0}{t_0} \times 100 \tag{4}$$

where ω_0, d_0, and t_0 are the initial weight, diameter, and thickness, while ω_f, d_f, and t_f are the weight, diameter and thickness after sintering. The ratio between diameter and thickness changes or the k factor was calculated using equation (5), to quantify the anisotropy of shrinkage during sintering:

$$k = \frac{d_v}{t_v} \tag{5}$$

The presence of residual carbonates on the surface of pellets prepared with unrinsed and rinsed Bioglass® powder was investigated using scanning electron microscopy (SEM). SEM (S-4700, Hitachi, Tokyo, Japan) was operated in high vacuum mode at 2 kV. Samples were Pt coated using a sputter coater (K575X, Quorum Technologies, Lewes, DE, USA).

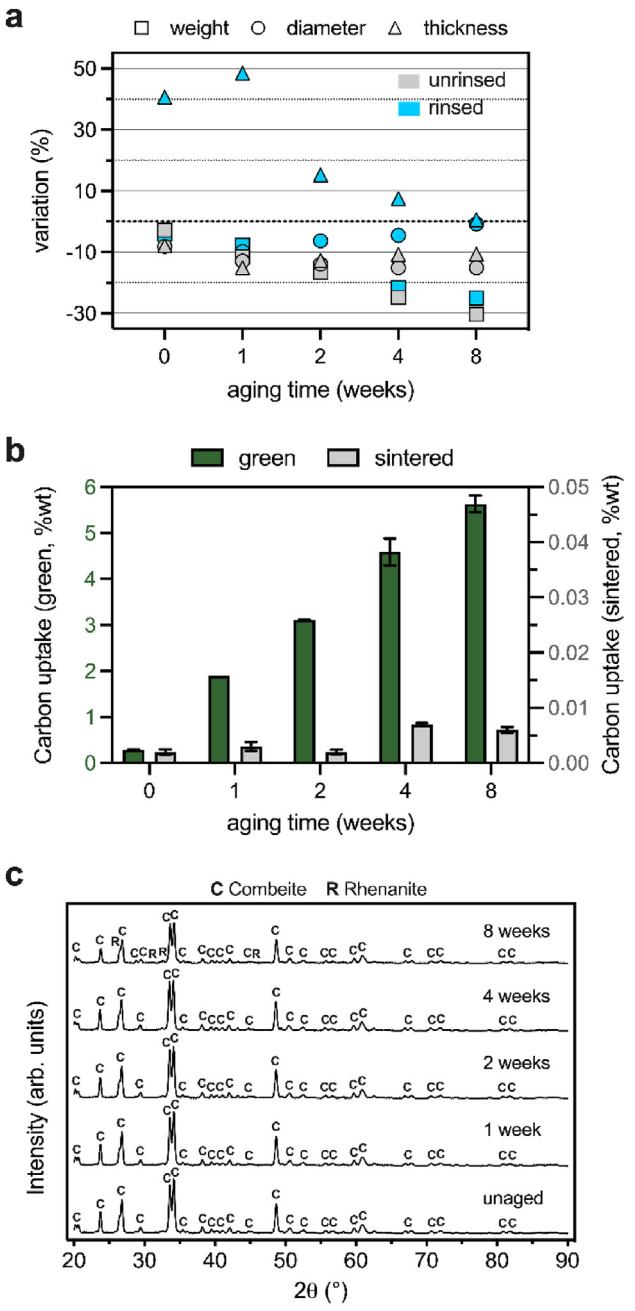

Fig. 2 – Characterization of the pellets. (a) Weight, diameter, and thickness changes versus aging time for pellets made with unrinsed (grey) and rinsed (blue) powders. (b) Carbon uptake versus aging time for green and sintered pellets. (c) XRD patterns of sintered pellets prepared with unaged (pristine) and aged (1, 2, 4, and 8 weeks) Bioglass® powders. (■) $Na_2Ca_2Si_3O_9$ (Combeite, PDF 98-006-0502); (●) $CaNaO_4P$ (Rhenanite, PDF 98-003-5629).

2.6. *Optimization of the fabrication process replicability*

Experiments were conducted to investigate the reproducibility of the sintering process. The aging time and drying

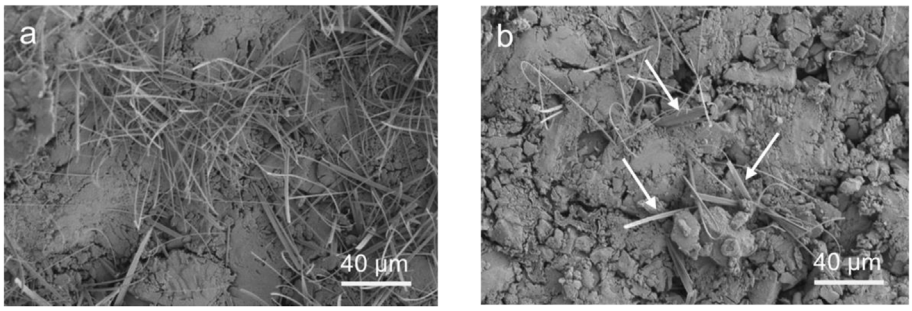

Fig. 3 – SEM micrographs of pellets made with (a) unrinsed and (b) rinsed powders aged for 8 weeks. The arrows in b indicate the presence of residual carbonates after the rinsing process.

temperature were established as controllable inputs, while the carbon and moisture content were identified as uncontrollable parameters of the sintering process. The density of the sintered pellets was chosen as the measurable output.

Twelve conditions were evaluated using aged (1 and 2 weeks) and unaged powder samples that were either undried or dried at three different temperatures (40 °C, 60 °C, and 100 °C). For each test, the carbon content after aging and the moisture content after drying were measured. Then, each powder sample was pressed into a pellet, and densities were calculated after sintering at 1035 °C for 1 h using equation (5). The results obtained were evaluated using Minitab® statistical software.

3. Results

3.1. *Chemical-physical and morphological characterization of BG powders and pellets*

A monotonic mass increase with aging was observed for all powders, with values up to +30.11% after 8 weeks. The corresponding carbon uptake is shown in Fig. 1a, showing an increase in carbon content from negligible values to 5.63% in 8 weeks. These results are proportional to the mass uptake and are likely to be related to the formation of carbonate species.

The XRD patterns of the powders are shown in Fig. 1b. The unaged sample showed a diffraction pattern typical of an amorphous material. The XRD results confirm that the aging treatment resulted in the nucleation of calcium carbonate (calcite, PDF 98-001-8166, 98-015-8257, and 98-016-9932, and aragonite, PDF 98-005-6090 and 98-016-9893), which was detected at all aging times. Sodium bicarbonate ($NaHCO_3$, PDF 98-001-8183, 98-002-3868 and 98-002-6933) was also detected at all aging time points, while sodium carbonate (Na_2CO_3, PDF 98-016-8129) was observed after 4 weeks of aging.

Fig. 2a shows the weight, diameter, and thickness variations of sintered pellet samples prepared with the aged powders. For the pellets prepared with unrinsed powders, the weight loss of the pellets increased with aging for the same initial weight (w = 1.32 ± 0.01 g) and dimensions (d = 15.71 ± 0.05 mm and t = 3.61 ± 0.14 mm), from 2.8% for unaged powder to 30.3% for powder aged for 8 weeks. These variations are likely due to the decomposition of the carbonates during sintering. While diameter variations increased with aging time, no reliable trend was observed for thickness variations. LECO analysis detected a negligible amount of carbon after sintering regardless of aging time (Fig. 2b), confirming the decomposition of the carbonate and suggesting that residue remains after sintering. XRD analysis performed on the same pellets confirmed the absence of crystalline phases attributable to carbonate species (Fig. 2c). However, while only combeite ($Na_2Ca_2Si_3O_9$, PDF 98-006-0502) was detected on the surface of the samples aged up to 4 weeks, traces of rhenanite ($CaNaO_4P$, PDF 98-003-5629) were also identified after 8 weeks. The XRD patterns of the sintered powders aged at different times are almost identical, indicating that crystallization of BG occurred during sintering and all pellets had similar compositions after sintering (Fig. 2c).

Weight, diameter, and thickness changes were also measured on pellets prepared from rinsed and dried powders (Fig. 2a, blue). A decrease in weight with increasing aging time was observed, from 4.1% for the unaged powder up to 25.0% for the powder aged for 8 weeks. Conversely, diameter and thickness variations decreased by 0.8% and 0.6% for the

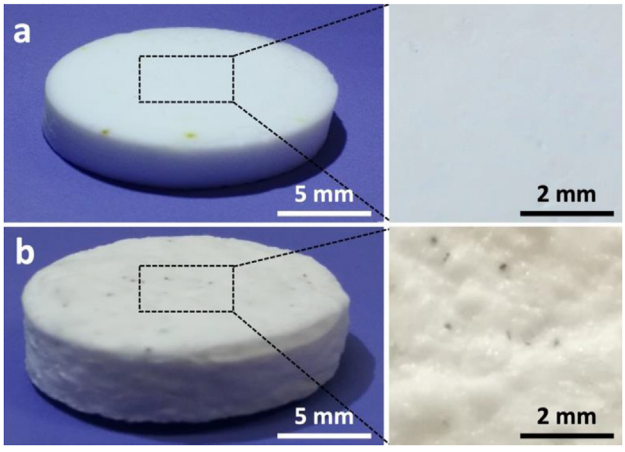

Fig. 4 – Low magnification photographs (left) and stereomicroscope images (right) of pellets made from (a) unrinsed and (b) rinsed powders that were aged for 8 weeks.

powder aged for 8 weeks. The weight decrease observed during the sintering of the pellets produced with the rinsed powders suggests the presence of residual moisture and carbonates after the rinsing and drying process. This assumption was investigated using SEM micrographs of a pellet produced with rinsed powder and aged for 8 weeks. The micrographs shown in Fig. 3 confirm the presence of residual carbonates even after the rinsing process. The sintering process also resulted in a morphological change with an increase in surface roughness compared to the smooth surface observed in the pellets prepared with the unrinsed powders (Fig. 4).

The shrinkage anisotropy factor k was evaluated on sintered pellets prepared with aged powders using equation (5). The results for unrinsed and unaged powders showed an isotropic contraction with a k value of 1.03 (Fig. 5a, point **A**). Thereafter, shrinkage anisotropy increased with aging, with a k-value as high as 1.41 for the pellet prepared with the powder aged for 8 weeks (Fig. 5a, point **E**). Conversely, the pellets made with the unaged powder showed anisotropic shrinkage during sintering (with $k < 0$), as shown in Fig. 5b, which appears to decrease with increasing carbon content.

Moreover, the pellets prepared with unrinsed powders show decreasing density values with aging, from 2.53 g cm^{-3} for the 1-week aged sample to 1.91 g cm^{-3} for the 8 weeks aged sample. Conversely, lower but more consistent density values (1.42 ± 0.10 g cm^{-3}) were obtained for the pellets prepared with the rinsed powders.

3.2. *Optimization of the fabrication process replicability*

The result of the experiment is summarized in Fig. 6. The density of each sintered pellet was plotted as a function of the moisture content found in each sample after drying at specific temperatures (undried, 40, 60, and 100 °C). Overall, the trend shows that the density of the pellet decreases with aging time and residual moisture content.

4. Discussion

4.1. *Nucleation of carbonates during aging*

It is well known that bioactive glass powders exhibit strong reactivity when exposed to atmospheric conditions, usually leading to carbonation of their surface, to an extent that depends on the exposed surface area (in the case of powders, on the granulometry of the particles). This highly reactive behavior has been described in detail for several bioactive glass formulations [17,18], with particular reference to the action of different carbonate entrapment, formation, and evolution mechanisms [19]. Among the main sources of carbonates, the adsorption of atmospheric CO_2 plays a fundamental role, together with carbonate species mechanically entrapped just below the surface of powder grains, both during powder milling and scaffold preparation [18]. In the present work, the mass and carbon uptake observed with increasing aging time can be associated with the formation of carbonates (Na_2CO_3 and $CaCO_3$) and hydrocarbonates ($NaHCO_3$) on the surface of the bioactive glass powders (Fig. 1a). These reactions are confirmed by XRD analysis,

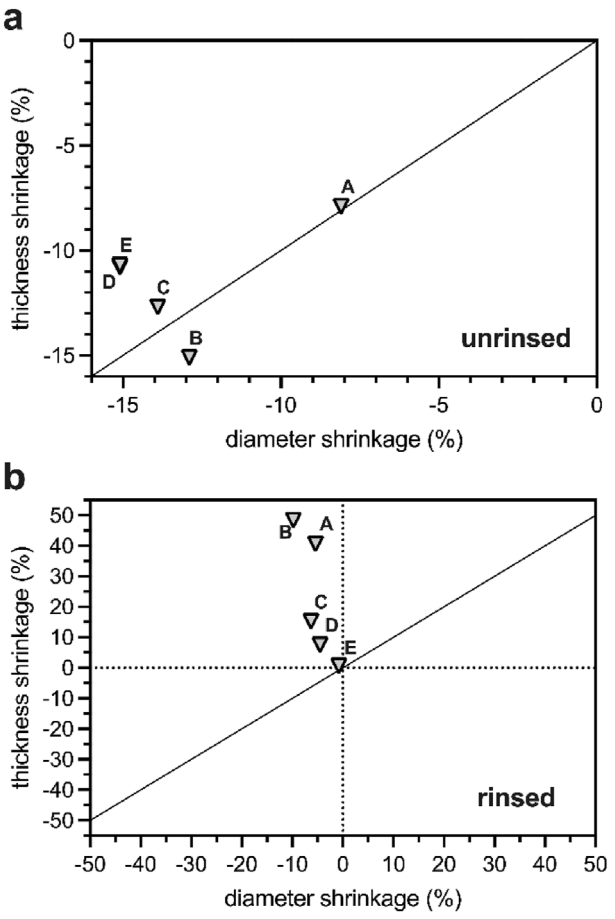

Fig. 5 – (a) Shrinkage of thickness versus diameter after sintering of pellets made with unrinsed powder. (b) Shrinkage of thickness versus diameter after sintering of pellets made with rinsed powder. The points represent powders aged for different lengths of time: (A) unaged, (B) 1, (C) 2, (D) 4, and (E) 8 weeks. The angle bisector corresponds to the isotropic line (k = 1).

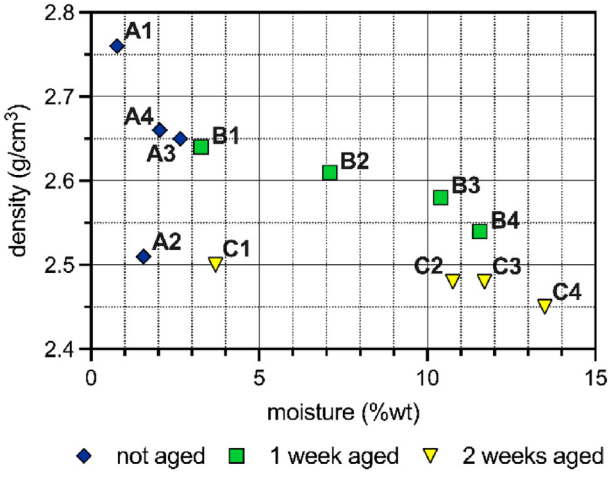

Fig. 6 – Density of sintered pellet versus moisture content of the powder. An unaged, B 1 week aged, C 2 weeks aged powder dried at 1100 °C, 2 60 °C, 3 40 °C, and 4 undried.

which shows an increasing intensity of the peaks associated with crystalline carbonate phases with increasing aging time (Fig. 1b). These results are consistent with previous studies on bioactive glass-ceramic foam samples [16].

The weight loss observed when sintering pellets from aged powders can be related to the decomposition of carbonates and, to a lesser extent, to the evaporation of residual moisture during the sintering process (T = 1035 °C). A greater weight loss is observed with increasing aging time (i.e., samples with higher carbonate content). Therefore, samples with greater carbon uptake also exhibit the highest weight loss after sintering (Fig. 2a). However, the XRD and LECO analyses performed on the sintered pellets confirmed the absence of carbonate species for all aging times (Fig. 2b and c). The sintering process of the amorphous (as highlighted in Fig. 1b) BG powders mainly involved surface crystallization due to their small particle size [20,21] and resulted in the formation of crystalline combeite phase ($Na_2Ca_2Si_3O_9$) with a limited presence of rhenanite ($CaNaO_4P$) only in aged powders (Fig. 2c). The same crystalline phases have been observed in previous studies on sintered bioactive glasses [16,22,23]. Crystallization begins when the sintering temperature reaches the glass-in-glass phase separation temperature (T_s = 580 °C) and the crystallization temperature (T_c = 610 °C). The amorphous phase remains predominant until 620 °C, when $Na_2Ca_2Si_3O_9$ nucleation starts [21]. Then the structure becomes mainly crystalline when the sintering temperature is increased up to 1000 °C, where complete crystallization of $Na_2Ca_2Si_3O_9$ with small amount of $CaNaO_4P$ is observed.

SEM observations (Fig. 3) confirmed the presence of residual carbonates on the surface of the pellet prepared with the 8-week aged and rinsed powder. The presence of residual carbonates and potential moisture after the rinsing and drying process resulted in weight reduction after sintering. This may be attributed to the low solubility of $CaCO_3$ (0.0013 g l^{-1} at 20 °C) compared to Na_2CO_3 and $NaHCO_3$ (220 g l^{-1} and 96 g l^{-1} at 20 °C, respectively). Based on the Shrinkage Core Model, in which solid particles are consumed inward starting from the outer layers [24], pellet shrinkage can be related to the thermal decomposition of carbonates. This phenomenon occurs at or above the thermal decomposition temperature. During the sintering process, carbonates decompose at different temperatures releasing CO_2 and are gradually consumed, according to the following equations:

$$CaCO_3 \rightarrow CaO + CO_2 \quad (6)$$

$$Na_2CO_3 \rightarrow Na_2O + CO_2 \quad (7)$$

$$2NaHCO_3 \rightarrow Na_2CO_3 + H_2O + CO_2 \quad (8)$$

The voids between the bioactive glass particles allow the release of CO_2, which leads to a reduction in the pellet volume and shrinkage of the pellets. This behavior is confirmed by the trends shown in Fig. 2a for pellets made with aged powders, which show an increase in diameter shrinkage with longer aging times.

In contrast to the observations reported by Bretcanu et al. [25], the variations in diameter were slightly larger than in thickness for pellets made from unrinsed powders. This resulted in anisotropic shrinkage of the pellet, which increased with aging time, as shown in Fig. 5a. Only the sample prepared with unaged powder showed isotropic shrinkage after the sintering process. This result confirms that an uncontrolled amount of carbonate species on the surface of bioactive glass powders can affect the reproducibility of the sintering process. Moreover, the shrinkage behavior after sintering the pellets prepared from aged and rinsed powders was also anisotropic, as shown in Fig. 5a and b. However, in this case, the pellets prepared with rinsed powders showed a larger thickness increase than the unrinsed powders. The overall greater tendency of the sample thickness to either decrease less than the diameter or even to increase can be attributed to the main phenomenon driving CO_2 release during sintering, *i.e.*, outward diffusion followed by desorption, which is characterized by a strong directional dependance: diffusion is indeed faster the larger the surface to volume ratio, and it occurs preferentially in the normal direction through the largest available surface area (the circular footprints of the pellets produced in this work). Moreover, since the shape factor of the pellets is highly directional (thickness > > diameter), diffusion in the perpendicular (radial) direction can be almost neglected. This behavior indicates that large amounts of carbonates remain in the powders, especially in the rinsed powders, suggesting unsuccessful carbonate removal. However, the anisotropy factor observed during the sintering of the pellets prepared with the rinsed powders decreased with aging time.

The decrease in density of the pellets produced with the unrinsed powders is due to the increase in carbonate and residual moisture content with aging time. Thermal decomposition of the carbonates and moisture evaporation during the sintering process resulted in an increase in porosity in the pellets. Conversely, more constant density values were measured in pellets produced from aged and subsequently rinsed powders. Thus, a constant rinsing process may reduce the variation in sintering shrinkage between samples.

4.2. *Effect of carbonates and moisture on sintering*

The tests performed with both rinsed and unrinsed powder samples confirm that the presence of carbonates counteracts pellet shrinkage, resulting in limited contraction during sintering. Surprisingly, high residual moisture content also led to a non-negligible swelling of the pellets and thus to an increase in volume during short aging times, contrary to what is reported in the literature [18,19,26]. Therefore, carbonates and relatively high moisture contents seem to cause a synergistic effect in foaming during sintering, leading to significant variations that may hinder the reproducibility of the process if not properly controlled or monitored.

After sintering, a general decrease in pellet density with aging was observed. Also, this behavior could be due to the equilibrium between the carbonate content and the residual moisture, which, if not completely dried, especially after rinsing, tends to hydrate amorphous carbonate (ACC) species [27] and transform them into more thermally stable crystalline forms within the surface layers of the BG powder grains [28]. The higher thermal stability of the hydrated carbonates thus prevents CO_2 release during the initial, relatively low temperature phases of the sintering process. Consequently, it

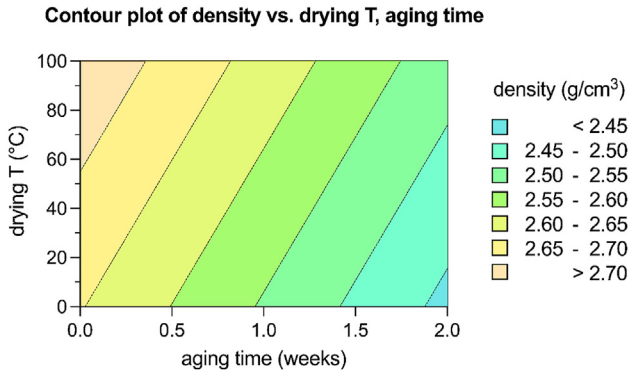

Fig. 7 – Contour plot of density as a function of aging time and drying temperature.

enhances their effect during pellet foaming, greatly reducing density after sintering. Accordingly, lower density values were obtained for powders with higher carbon content and similar residual moisture (*e.g.*, Fig. 6, points B4 and C3) and for powders with similar carbon content but higher residual moisture. Thus, the sintered pellets prepared with unaged powder dried at 100 °C (Fig. 6, point A1), were the only ones that approached the theoretical density of Bioglass® ($\rho_{Bioglass}$ = 2.7 g cm^{-3}) [29], due to the dual effect of relatively prolonged low heating, which both removes residual moisture and contributes to the decomposition of carbonates and CO_2 release prior to pellet formation and sintering.

Moreover, the greater reactivity of ACCs with water compared to crystalline carbonates could explain the stronger influence of this behavior in unaged and poorly aged powders (Figs. 5 and 6). At the same time, it is almost negligible for powders that have been exposed to the atmosphere for a longer time (*i.e.*, powders on whose surface carbonate nucleation and crystallization already cover most of the grains, as shown in Fig. 1b). Another negative effect on densification is the presence of $NaHCO_3$, the content of which increases as the powder ages. During sintering, $NaHCO_3$ gradually decomposes into Na_2CO_3, water and CO_2, as shown in equation (8). While the released CO_2 directly contributes to foaming, the release of additional water molecules from the pellets further slows down densification, resulting in a lower density after sintering.

The contour plot shown in Fig. 7 illustrates how aging time and drying temperature affect sample density after sintering. It shows that a specific range of density can be achieved by acting on the controllable factors of the system. Thus, a controlled amount of carbonates and residual moisture allows consistent results after sintering. Low carbon and moisture contents are required to optimize sintering and achieve the theoretical density of Bioglass® ($\rho_{Bioglass}$ = 2.7 g cm^{-3}), as shown by the darkest area of the contour plot. This can possibly only be achieved by minimizing the aging process and drying the powders at about 100 °C. However, for 45S5 Bioglass®, it must be taken into account that other process parameters are also fundamental for effective densification, such as a sufficiently high applied pressure [30] or the sintering temperature [31], the latter enabling secondary sintering and densification [25,32].

5. Conclusions

This study investigated the impact of aging on the sintering of bioactive glass powder. Aging of Bioglass® powder leads to the formation of carbonates (Na_2CO_3 and $CaCO_3$) and hydrocarbonates ($NaHCO_3$) when in contact with atmospheric CO_2 and humidity. While water evaporates and carbonates decompose without leaving residues after sintering, the presence of these compounds can affect the sintering behavior of the Bioglass® powders, thus affecting the reproducibility of the sintering and the control of the final material properties.

The optimization results show that a controlled balance between carbonates and residual moisture content can achieve constant sintering. Furthermore, the theoretical density of Bioglass® ($\rho_{Bioglass}$ = 2.7 g cm^{-3}) could only be achieved by minimizing the aging process and drying the powder to allow complete evaporation of the residual moisture, provided that the sintering temperature or applied pressure are sufficiently high. These results highlight the importance of proper raw material handling, processing and storage to prevent powder aging and improve the reproducibility of sintering.

In addition to the effect of aging and the presence of carbonates and moisture on the sintering of Bioglass® powder, changes in surface chemistry may also affect the behavior of the powders when used in various applications (*e.g.*, dissolution and pH of suspensions when mixed with binders or solvents). Therefore, further studies would be valuable to better understand the effects of aging and carbonate formation on the properties of Bioglass® particles.

Declaration of competing interest

The authors declare that they have no known competing financial interests or personal relationships that could have appeared to influence the work reported in this paper.

Acknowledgments

The authors would like to acknowledge the contribution of Jean-Paul Nadeau, Shirley Mercier and Patrick England for their support in the experimental work.

Appendix A. Supplementary data

Supplementary data to this article can be found online at https://doi.org/10.1016/j.jmrt.2023.06.204.

REFERENCES

[1] Boccardi E, Ciraldo FE, Boccaccini AR. Bioactive glass-ceramic scaffolds: processing and properties. MRS Bull 2017;42:226–32. https://doi.org/10.1557/mrs.2017.28.

[2] Boccardi E, Melli V, Catignoli G, Altomare L, Jahromi MT, Cerruti M, et al. Study of the mechanical stability and bioactivity of Bioglass® based glass-ceramic scaffolds produced via powder metallurgy-inspired technology. Biomed Mater 2016;11:015005. https://doi.org/10.1088/1748-6041/11/1/015005.
[3] Jones JR. Reprint of: review of bioactive glass: from Hench to hybrids. Acta Biomater 2015;23:S53–82.
[4] Amini AR, Laurencin CT, Nukavarapu SP. Bone tissue engineering: recent advances and challenges. Crit Rev Biomed Eng 2012;40:363–408. https://doi.org/10.1615/CritRevBiomedEng.v40.i5.10.
[5] Jones JR, Brauer DS, Hupa L, Greenspan DC. Bioglass and bioactive glasses and their impact on healthcare. Int J Appl Glass Sci 2016;7:423–34. https://doi.org/10.1111/ijag.12252.
[6] El-Rashidy AA, Roether JA, Harhaus L, Kneser U, Boccaccini AR. Regenerating bone with bioactive glass scaffolds: a review of in vivo studies in bone defect models. Acta Biomater 2017;15:1–28. https://doi.org/10.1016/j.actbio.2017.08.030.
[7] Chen QZ, Efthymiou A, Salih V, Boccaccini AR. Bioglass®-derived glass-ceramic scaffolds: study of cell proliferation and scaffold degradation in vitro. J Biomed Mater Res, Part A 2008;84:1049–60. https://doi.org/10.1002/jbm.a.31512.
[8] Chen Q, Mohn D, Stark WJ. Optimization of Bioglass® scaffold fabrication process. J Am Ceram Soc 2011;94:4184–90. https://doi.org/10.1111/j.1551-2916.2011.04766.x.
[9] Bellucci D, Cannillo V, Sola A, Chiellini F, Gazzarri M, Migone C. Macroporous Bioglass®-derived scaffolds for bone tissue regeneration. Ceram Int 2011;37:1575–85. https://doi.org/10.1016/j.ceramint.2011.01.023.
[10] Esslinger S, Gadow R. Additive manufacturing of bioceramic scaffolds by combination of FDM and slip casting. J Eur Ceram Soc 2020;40:3707–13. https://doi.org/10.1016/j.jeurceramsoc.2019.10.029.
[11] Ma Z, Xie J, Shan XZ, Zhang J, Wang Q. High solid content 45S5 Bioglass®-based scaffolds using stereolithographic ceramic manufacturing: process, structural and mechanical properties. J Mech Sci Technol 2021;35:823–32. https://doi.org/10.1007/s12206-021-0144-9.
[12] Baino F, Fiume E, Barberi J, Kargozar S, Marchi J, Massera J, et al. Processing methods for making porous bioactive glass-based scaffolds—a state-of-the-art review. Int J Appl Ceram Technol 2019;16:1762–96. https://doi.org/10.1111/ijac.13195.
[13] Ghalayani Esfahani A, Soleimanzade M, Campiglio CE, Federici A, Altomare L, Draghi L, et al. Hierarchical microchannel architecture in chitosan/bioactive glass scaffolds via electrophoretic deposition positive-replica. J Biomed Mater Res, Part A 2019;107:1455–65. https://doi.org/10.1002/jbm.a.36660.
[14] Henkel J, Woodruff MA, Epari DR, Steck R, Glatt V, Dickinson IC, et al. Bone regeneration based on tissue engineering conceptions — a 21st century perspective. Bone Res 2013;1:216–48. https://doi.org/10.4248/BR201303002.
[15] Charbonneau C, Vanier F, Lefebvre L. Stability of bioactive bone graft substitutes exposed to different aging and sterilization conditions. Int J Ceram Eng Sci 2020;2:152–61. https://doi.org/10.1002/ces2.10047.
[16] Menci PF, Mari A, Charbonneau C, Lefebvre LP, De Nardo L. Aging of bioactive glass-based foams: effects on structure, properties, and bioactivity. Materials 2019;12:1–13. https://doi.org/10.3390/ma12091485.
[17] Cerruti M, Morterra C. Carbonate formation on bioactive glasses. Langmuir 2004;20:6382–8. https://doi.org/10.1021/la049723c.
[18] Blaeß C, Müller R. Sintering and foaming of bioactive glasses. J Am Ceram Soc 2022;105:6616–26. https://doi.org/10.1111/jace.18626.
[19] Müller R, Behrens H, Agea-Blanco B, Reinsch S, Wirth T. Foaming species and trapping mechanisms in barium silicate glass sealants. Adv Eng Mater 2022;24:2100445. https://doi.org/10.1002/adem.202100445.
[20] Massera J, Fagerlund S, Hupa L, Hupa M. Crystallization mechanism of the bioactive glasses, 45S5 and S53P4. J Am Ceram Soc 2012;95:607–13. https://doi.org/10.1111/j.1551-2916.2011.05012.x.
[21] Contreras Jaimes AT, de Pablos-Martín A, Hurle K, Martins de Souza e Silva J, Berthold L, Kittel T, et al. Deepening our understanding of bioactive glass crystallization using TEM and 3D nano-CT. J Eur Ceram Soc 2021;41:4958–69. https://doi.org/10.1016/j.jeurceramsoc.2021.02.051.
[22] Hills AWD. The mechanism of the thermal decomposition of calcium carbonate. Chem Eng Sci 1968;23:297–320. https://doi.org/10.1016/0009-2509(68)87002-2.
[23] Clupper DC, Mecholsky JJ, Latorre GP, Greenspan DC. Sintering temperature effects on the in vitro bioactive response of tape cast and sintered bioactive glass-ceramic in Tris buffer. J Biomed Mater Res 2001;57:532–40. https://doi.org/10.1002/1097-4636(20011215)57:4<532::AID-JBM1199>3.0.CO;2-3.
[24] Mohamed M, Yousuf S, Maitra S. Decomposition study of calcium carbonate in cockle shell. J Eng Sci Technol 2012;7:1–10.
[25] Bretcanu O, Chatzistavrou X, Paraskevopoulos K, Conradt R, Thompson I, Boccaccini AR. Sintering and crystallisation of 45S5 Bioglass® powder. J Eur Ceram Soc 2009;29:3299–306. https://doi.org/10.1016/j.jeurceramsoc.2009.06.035.
[26] Agea-Blanco B, Reinsch S, Müller R. Sintering and foaming of barium silicate glass powder compacts. Front Mater 2016;3:1–10. https://doi.org/10.3389/fmats.2016.00045.
[27] Radha AV, Navrotsky A. Direct experimental measurement of water interaction energetics in amorphous carbonates MCO 3 (M = Ca , Mn , and Mg) and implications for carbonate crystal growth. Cryst Growth Des 2015;15:70–8. https://doi.org/10.1021/cg500878w.
[28] Albéric M, Bertinetti L, Zou Z, Fratzl P, Habraken W, Politi Y. The crystallization of amorphous calcium carbonate is kinetically governed by ion impurities and water. Adv Sci 2018;5:1701000. https://doi.org/10.1002/advs.201701000.
[29] Hench LL, Wilson J. An introduction to bioceramics. World Sci 1993:41–75. https://doi.org/10.1142/9781908977168_0021.
[30] Guillon O, Cao S, Chang J, Wondraczek L, Boccaccini AR. Effect of uniaxial load on the sintering behaviour of 45S5 Bioglass® powder compacts. J Eur Ceram Soc 2011;31:999–1007. https://doi.org/10.1016/j.jeurceramsoc.2010.12.031.
[31] Blaeß C, Müller R, Poologasundarampillai G, Brauer DS. Sintering and concomitant crystallization of bioactive glasses. Int J Appl Glass Sci 2019;10:449–62. https://doi.org/10.1111/ijag.13477.
[32] Lefebvre L, Gremillard L, Chevalier J, Zenati R, Bernache-assolant D. Sintering behaviour of 45S5 bioactive glass. Acta Biomater 2008;4:1894–903. https://doi.org/10.1016/j.actbio.2008.05.019.